Flow Turbulence Combust (2012) 88:19–44
DOI 10.1007/s10494-011-9353-0

Large Eddy Simulation of Transitional Separated Flow over a Flat Plate and a Compressor Blade

Sylvain Lardeau · Michael Leschziner · Tamer Zaki

Received: 10 December 2010 / Accepted: 20 May 2011 / Published online: 2 July 2011

Abstract The ability of Large-Eddy Simulation (LES) to predict transitional separation bubbles is investigated, with particular emphasis being placed on the response to free-stream-turbulence. The principal objective is to quantify the penalties, relative to Direct Numerical Simulations (DNS), that arise from the coarser resolution and the use of subgrid-scale models. Two flow configurations are considered: a flat-plate boundary layer, subjected to different free-stream-turbulence levels, ranging from 0 to 2% (at the point of separation), and the flow over a compressor blade at 0 and 3.25% turbulence levels. For both cases, results are compared with DNS data. A number of challenges associated with the use of LES in transitional flows are addressed, including the representation of the decay of free-stream turbulence and the mesh resolution needed for a correct description of the growth of instability waves in the early stage of transition.

Keywords Large Eddy Simulation (LES) · Laminar separation · Bypass transition · Turbulent reattachment · Turbomachine blades

1 Introduction

Transition is a feature of virtually all practical flows around streamlined solid bodies. Of these, external aerodynamic and turbomachinery flows are exceptional, in so far

S. Lardeau (✉) · M. Leschziner
Department of Aeronautics, Imperial College London, London, UK
e-mail: s.lardeau@imperial.ac.uk, sylvainlardeau@gmail.com

M. Leschziner
e-mail: mike.leschziner@imperial.ac.uk

T. Zaki
Department of Mechanical Engineering, Imperial College London, London, UK
e-mail: t.zaki@imperial.ac.uk

as the transition process is usually of major importance to the primary operational characteristics of the component around which the flow develops. Transition may be natural or of the bypass type, and it may occur in the boundary layer or following laminar separation. Correspondingly, the fundamental flow physics at play vary greatly, and this poses a major challenge to any simulation and modelling approach, especially one that is rooted in a statistical framework. In vanishingly low free-stream turbulence, the dominant transition mechanism is associated with the inflectional profile in the early stage of the separation, similar to Kelvin–Helmholtz instability occurring in free-shear layers [6]. This behaviour has been confirmed by DNS in 2D flows, (e.g. [23]). When free-stream disturbances are introduced, the transition process in the separated shear layer is altered dramatically. Thus, Λ-vortices appear early in the separated region [2], even at low free-stream-turbulence levels. For higher values of the free-stream-turbulence intensity, Tu, the transition in the separated shear-layer is preceded by a bypass-transition process in the attached boundary layer.

The fluid mechanics of the flow around compressor and turbine blades are especially complex, due to leading-edge and suction-side curvature, strong pressure gradients and the complex nature of the free-stream or passage flow above the boundary layer [11]. In low-pressure stages of a turbomachine, the Reynolds number is relatively modest, and the flow may be transitional over a significant proportion of the blade, especially in a turbine stage. Transition thus frequently occurs on the aft part of the blade, encouraged by migrating wakes and free-stream turbulence. In very recent turbomachine designs, the number of blades is lower than in earlier configurations, in order to reduce weight, thus requiring an increase in loading on each blade. As a result, the suction-side boundary layer is more prone to separation, particularly in the compressor stage. The separated shear layer then usually becomes turbulent soon after separation and reattaches quickly, usually upstream of the trailing edge. The separation bubble formed as a consequence of this process alters the effective shape of the blade, thus degrading the blade's performance and increasing losses. The transition process is especially sensitive to free-stream turbulence, with increasing levels resulting in earlier reattachment and a reduction in the length of the recirculation bubble. This interaction is thus especially important to capture in any prediction procedure.

Most computations used in industrial design of turbomachines are based on the Reynolds-Averaged Navier–Stokes (RANS) approach. The need for a turbulence model to accommodate both separation-induced and bypass transition clearly constitutes a major challenge. For example, the pre-transitional state of the boundary layer typically features non-turbulent, predominantly one-component (streaky), fluctuations of substantial intensity, the effect of which on the transition process is very difficult to capture within a RANS framework [14]. Thus, models for transitional boundary layers require much ad-hoc tuning to achieve an acceptable match with experiments. This is, self-evidently, undesirable in an integrated design environment, where Computational Fluid Dynamics (CFD) is used as a truly predictive tool in a complex environment, rather than for validating laboratory flows. On the other hand, Direct Numerical Simulation (DNS) is computationally far too costly for engineering simulations. There is, therefore, considerable interest in exploring the capabilities and limitations of Large Eddy Simulations (LES) and hybrid methods, the latter combining LES and RANS, in turbomachine aero/thermodynamics, in general, and the prediction of transitional blade flows, in particular. The critical issue

is whether LES-based schemes, with their relatively coarse resolution and subgrid-scale models, are able to capture, with acceptable fidelity, the refined physics that transition involves.

In a typical transition scenario on a blade, a very thin boundary layer initially develops from its inception at a leading-edge stagnation line. In the presence of an adverse pressure gradient, immediately beyond the highly-curved leading edge, a thin laminar separation bubble may form. Both can only be captured with a fine near-wall grid, thus potentially negating the basic rationale of LES. The transition process itself involves the onset of instabilities and subsequent growth of perturbations within the boundary layer, whether with and without free-stream turbulence. An adequate representation of this growth is important to the objective of making LES a viable alternative to RANS as an industrial-design tool. When transition is provoked by free-stream turbulence, either before or after separation, the response of the boundary and free-shear layers to both the level of free-stream turbulence and its spectral features has to be accurately simulated in order to correctly capture the transition location and its spatial extent towards a fully turbulent state. In particular, the need for a subgrid-scale (SGS) model, and its inevitable interaction with important small-scale mechanisms, is a non-trivial issue in transitional flows, especially if subjected to high-frequency periodic perturbations.

The literature on the simulation of laminar separation followed by transition is dominated by DNS studies of flat-plate boundary layers, made to separate in a laminar state by means of suction/blowing or wall contouring and undergoing subsequent transition. The objective of most studies was to investigate a variety of fundamental aspects of the separation, transition and reattachment processes in the absence of free-stream turbulence. Examples include the studies of Alam and Sandham [2], Spalart and Strelets [26], Fasel and Postl [7], Marxen and Henningson [17] and Wissink and Rodi [27], the last focusing on the effects of periodic upstream oscillations. DNS applications that have examined the response of transition and separation to free-stream turbulence or turbulent wakes include those of Wissink and Rodi [28], Wu and Durbin [29] and Zaki et al. [31, 32]. LES studies of transitional flows are far rarer, presumably because of concerns about the penalties arising from low resolution and subgrid-scale modelling. A recent study by Monokrousos et al. [20] investigates the ability of LES to resolve bypass transition in a zero-pressure-gradient boundary layer on a flat plate subjected to a relatively high free-stream-turbulence intensity, with the emphasis of the study being placed on the delay of transition with the aid of linear feedback control. As regards resolution, in particular, the main conclusion is that the LES grid must be capable of resolving the long streaks preceding the transition to turbulent spots. This study demonstrates that the essential features of the transition process can then be captured at a resolution of around 10% of the equivalent DNS, provided close attention is paid to subgrid-scale modelling. In research by Yang and Voke [30] and Abdalla and Yang [1], LES was used to investigate transitional boundary layers separating, respectively, from a rounded and a square leading edge. In both cases, the dynamics of the separation bubble was found to be very sensitive to the geometrical conditions, as well as the inflow and the boundary conditions. More complex applications of LES to transitional separation from blades are reported by Michelassi et al. [19] and Roberts and Yaras [25]. Both show that LES gives a fair approximation of the respective DNS solutions, although the sources of the differences are not explored in detail.

The principal objective of this study is to explore in some detail the ability of LES to reproduce the DNS-resolved processes in transitional separation, subject to free-stream turbulence, in two geometries: a flat plate opposed by a contoured wall and a compressor blade. Details about the flow configurations are given in Section 2. Three subgrid-scale models are investigated, and these are summarised in Section 3, along with the computational methods. The results obtained for the flat plate and the compressor cases are then presented in Sections 4 and 5, respectively.

2 Flow Configurations

The flow geometries examined herein are shown in Fig. 1. In both cases, the flow is subjected to various levels of free-stream perturbations, as listed in Table 1, and laminar separation is observed in both configurations for at least one free-stream-turbulence level. The flat-plate case is similar to the configuration studied experimentally by Lou and Hourmouziadis [16] and numerically by Wissink and Rodi [28]. The inflow is prescribed 0.5 times of the "chord" length L upstream of the origin of the boundary layer, the "chord" in Fig. 1a being the plate length in the

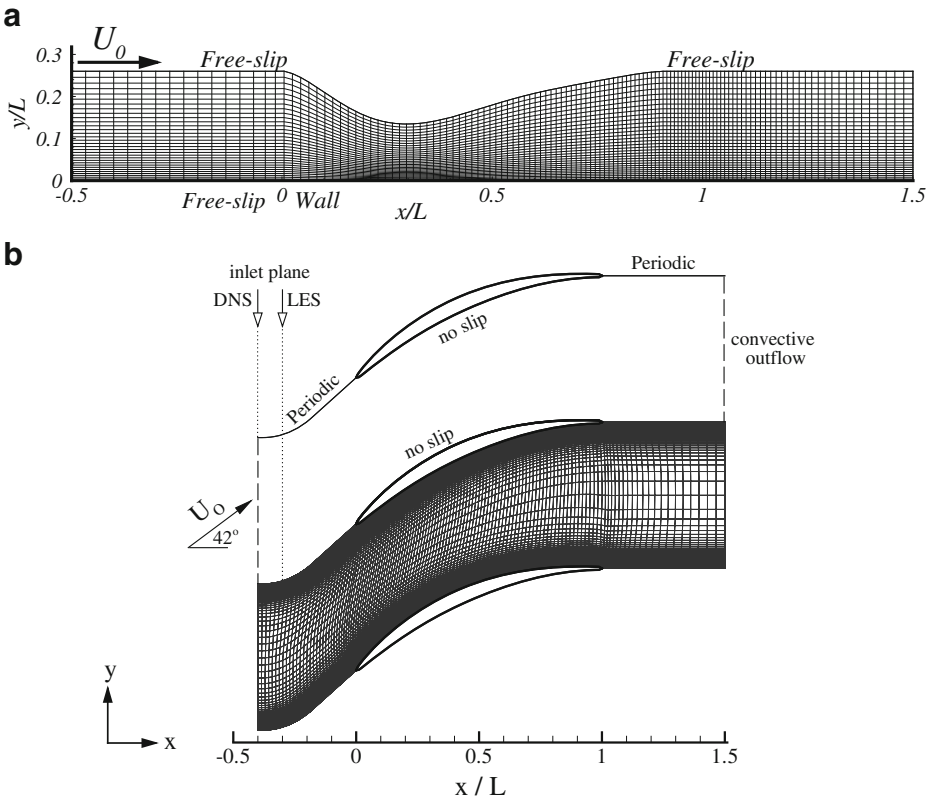

Fig. 1 Computational grid (every 4th grid point shown) and boundary conditions for **a** flat plate boundary layer with adverse pressure gradient and **b** V103 compressor blade

Table 1 Cases simulated and inflow parameters (*DHIT*: decaying homogeneous isotropic turbulence)

Case	Geometry	Tu (%)	Inflow
Case FP1	Flate plate	0	N.A.
Case FP2	Flate plate	1	Eq. 1
Case FP3	Flate plate	1	Eq. 2
Case FP4	Flate plate	1.5	Eq. 1
Case FP5	Flate plate	2	Eq. 1
Case Co1	Compressor	0	N.A
Case Co2	Compressor	3.25	DHIT from DNS [34]

experiments of Lou and Hourmouziadis [16] opposing the bump on the contoured wall. In the present study, the flat plate was extended to the computational outlet, $x/L = 1.5$, so as to allow the recovery needed to reach a fully turbulent state. The Reynolds number, based on the chord length L and the inflow velocity U_0, is 60,000. In the spanwise direction, the depth, constant for all cases, is $L_z = 0.12L$, similar to that used in previous DNS studies. The flow is covered with a grid of $(n_x, n_y, n_z) = (512, 128, 64)$, compared with the DNS resolution of $(n_x, n_y, n_z) = (1926, 230, 128)$ adopted by Wissink and Rodi [28]. Thus, the ratio of LES-to-DNS grid nodes is 7.5%.

The particular choice made in respect of the grid—also for the second geometry discussed below—is underpinned by two main rational arguments. First, as the principal objective of the study is to demonstrate economy, relative to DNS, without major loss of physical realism, the only sensible choice was of a grid that is much coarser than that required by DNS. A resource reduction by a factor of order 10 was judged to be a good starting point. A much lower saving, by use of a finer grid, did not seem worthwhile, in terms of deriving a statement on the viability of practical transition simulations. Second, preliminary simulations suggested that the resolution could be reduced further, but not much further. This then resulted in the particular choice of the grid, both for this case and the compressor-blade geometry. In effect, the grids used herein may be regarded as minimum-resolution recommendations for realistic solutions that capture all essential physical processes. Finer grid will simply reduce the difference to DNS, while coarser grids will result in serious loss of fidelity.

To avoid separation on the upper wall, and following Wissink and Rodi's strategy, a free-slip condition was imposed on this boundary. A similar condition was used along the lower boundary stretch $-0.5 < x/L < 0$ upstream of the flat-plate leading edge. At the outlet, a standard convective-outflow condition was imposed.

Statistics were collected after a settling-in time of $20L/U_0$ to ensure that the start-up vortex, created when the flow is accelerated in the convergent/divergent passage, had been evacuated. Statistics, including Reynolds-stress budgets, were then gathered over a period in excess of $40L/U_0$. More than 2,000 3D snapshots of the instantaneous-velocity field were also saved during this interval in order to perform a-posteriori statistical and dynamical-flow analysis (the latter utilized POD, and will be reported elsewhere).

The second geometry, Fig. 1b, is a compressor passage, designated *V103*. This was previously studied by Hilgenfeld and Pfitzner [10] and Zaki et al. [33]. The Reynolds number, based on the axial chord length L and inlet velocity U_0, is $Re = 138{,}500$. The blade-to-blade distance is $0.592L$. The inflow plane is located 0.4 times of the chord length upstream of the leading-edge of the compressor blade. The flow angle is 42° at the inlet. The LES mesh covering the single periodic passage comprises (512 ×

192 × 64) grid points in the streamwise, normal and spanwise directions, respectively. This compares with a DNS resolution of (1024 × 640 × 128) grid points—a LES-to-DNS ratio of 7.5%. It will be shown below that the resolution requirements are of major importance in the early transition region. One aspect of the challenge posed to LES by transitional boundary layers is the requirement that it should be able to correctly represent the disturbance-free, intermittently turbulent and the fully-turbulent regions of the flow. Therefore, it is important that the LES recovers the correct behaviour when the perturbation field vanishes. To demonstrate this ability, LES computations were performed for two sets of conditions: the main simulation was for an inflow turbulence intensity $Tu = 3.25\%$; the supplementary simulation was for vanishingly low inflow turbulence, undertaken in order to examine the behaviour of the model in the "laminar" limit, which is important in respect of the representation of the instability and growth of disturbances within the pre-transitional boundary layer. For the case of $Tu = 3.25\%$, the inflow perturbations were identical to those of the DNS study of Zaki et al. [33], including the spectral content of the inlet perturbations.

3 The LES Framework

3.1 Computational framework

The in-house numerical scheme STREAM-LES was used to solve the implicitly-filtered LES momentum and continuity equations for incompressible flow over a non-orthogonal, boundary-fitted mesh. The numerical strategy is based on the co-located finite-volume approach. In order to suppress unphysical oscillations, associated with pressure-velocity decoupling, the scheme includes a practice equivalent to that introduced by Rhie and Chow [24]. Within this framework, the fluxes are approximated by central differences, with a dynamic wiggle-detector [5] used to eliminate odd-even oscillations, and time-advancement utilized a fractional-step scheme within which the time-derivative was approximated by a third-order Gear scheme [8]. In this two-step process, the provisional velocity field resulting from advancing the solution with the flux operators is corrected by a pressure gradient, which is evaluated by projecting the provisional solution onto a divergence-free velocity field. To this end, the pressure is computed as a solution to the pressure-Poisson problem using a multigrid scheme. The STREAM-LES code, incorporating the above practices, has been used extensively in the writers' group for a wide range of LES studies over the past 10 years.

3.2 Inflow condition

One of the main challenges of simulating transitional flows in the turbomachinery environment is that transition is triggered by free-stream disturbances (e.g. of the Klebanoff type) and that the transition behaviour itself is very sensitive to the free-stream properties, specifically the turbulence intensity and the spectral composition. Several stability analyses have been performed for both attached and separated flows (e.g. [23]), and these have shown that both low- and high-frequency perturbations are needed to correctly trigger transition and turbulence. Thus, in the present simu-

lations, the perturbations also need to feature the wide range of scales necessary to induce transition realistically. Moreover, the decay of free-stream turbulence is likely to be reproduced correctly only if the spectral properties are realistically captured as the flow progresses downstream (Fig. 2). However, the correct representation of both short- and long-wavelength signals is very challenging in the LES environment, because of the unavoidable short-wave-length cut-off it introduces. In an effort to secure a high degree of fidelity, perturbations with prescribed spectra are imposed at the inlet in simulations with free-stream turbulence (Table 1). Two approaches have been used. First, following Brandt et al. [3], a state of quasi-isotropic and homogeneous perturbations was approximated using the modified von Kàrmàn spectrum:

$$E(\kappa) = \frac{2}{3}\frac{a(\kappa\mathscr{L})^4}{(b+(\kappa\mathscr{L})^2)^{17/6}}\mathscr{L} \tag{1}$$

with $a = 1.606$, $b = 1.35$ and the integral length-scale $\mathscr{L}$ given by $\mathscr{L} = 1.8/\kappa_p$, with κ_p being the wave number of maximum energy. The generic energy spectrum obtained using Eq. 1 is shown on Fig. 2a. The other formulation investigated was proposed by Ossia and Lesieur [22], and features a more pronounced "peak" in the spectrum. This is given by:

$$E(\kappa) = \frac{1}{\kappa_p}\left(\frac{\kappa}{\kappa_p}\right)^s \exp\left[-\frac{s}{2}\left(\frac{\kappa}{\kappa_p}\right)^2\right] \tag{2}$$

where s is a parameter controlling the slope of the low-wavenumber range. For the present simulations, the value of κ_p has been fixed at $0.015/L$, but preliminary studies on a smaller domain have not shown a significant sensitivity to this parameter. A typical spectrum obtained using Eq. 2 is also shown on Fig. 2a. The argument for using two different spectra is that, in experiments, the energy of the large-scale structures is more easily varied than the small-scale ones. Following Wissink and Rodi [28],

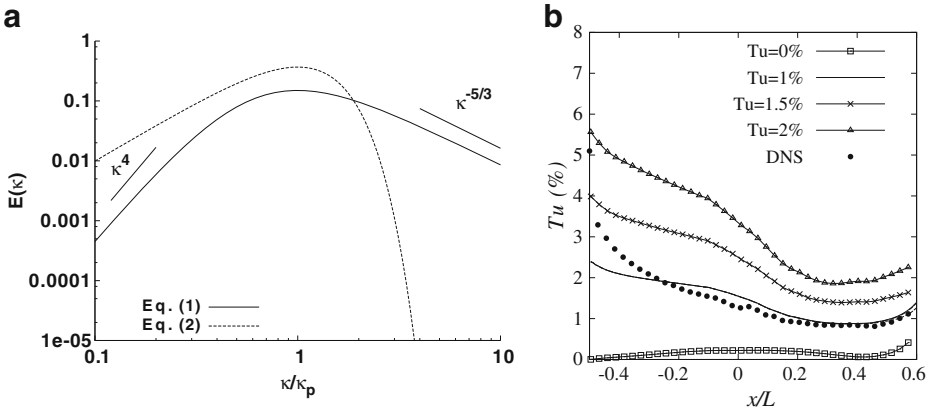

Fig. 2 **a** Energy spectra of the inflow free-stream turbulence, prescribed by Eqs. 1 and 2, and **b** decay of free-stream turbulence upstream of the flat-plate leading-edge

the turbulence intensity is recorded at $y/L = 0.065$, and comparisons between present LES Results and DNS data are shown in Fig. 2b. For the, nominally, 0% turbulence case, the LES returns a very low level of fluctuations just downstream of the flat-plate leading edge (around $x/H = 0$), possibly due to a combination of minor numerical wiggles and physical oscillations induced by the downstream flow. These fluctuations have no observable effect on the transition process. For $Tu = 1\%$, all SGS models (see next sub-section) return exactly the same behaviour upstream of the leading-edge (the different curves are not distinguishable on Fig. 2b), a result which is not surprising, as the subgrid-scale eddy viscosity is negligible in this region. It is important to point out that the turbulence intensity at the leading edge depends on the simulated decay characteristics in the free stream, starting from the nominal value prescribed at the inlet. Thus, to achieve the same level of Tu at the leading edge in the LES and benchmark DNS, the level of turbulence intensity prescribed at the inlet plane in the former had to be different to that in the latter. The differences between the two cases are only substantial close to the inlet, where the decay is much higher in the DNS than in the LES, possibly due to the high-aspect-ratio grid used in the former upstream of the leading edge. However, at the point of separation (occurring around $x/L = 0.385$), the values are identical, and in the following, the value of Tu measured at this point is therefore used as a reference, rather than the value at the inlet.

3.3 Subgrid-scale modelling

Several SGS models display, or have been claimed to possess, transition-prediction capabilities. However, there is no firm evidence to support any one model over others, except for the fact that the constant-coefficient Smagorinsky model has inferior properties because of its excessive damping and the finite subgrid-scale viscosity it yields in laminar conditions. The models used herein are based on the eddy-viscosity concept, for which the deviatoric part of the stress tensor τ_{ij}^* can be expressed as:

$$\tau_{ij}^* = -2\nu_t \overline{S}_{ij} \tag{3}$$

and $\overline{S}_{ij}$ is the filtered strain-rate tensor. The eddy-viscosity, ν_t, is here approximated by means of one of three models, namely the dynamic Smagorinsky model (DSM) of Germano et al. [9] with Lilly's [15] modifications, the mixed-time-scale (MTS) model of Inagaki et al. [12] and the Wall-Adapted Local Eddy-Viscosity (WALE) model of Nicoud and Ducros [21]. While the last is neither a dynamic model nor yielding a vanishing eddy viscosity in non-turbulent flows remote from a wall, it is claimed to give the correct asymptotic decay of the viscosity towards zero as the wall is approached, in contrast to the (almost equally) simple constant-coefficient Smagorinsky model. It is therefore a credible candidate for transitional boundary layers, at least if transition occurs while the flow is attached.

In the MTS model, the eddy-viscosity is linearly related to a *test-filtered* subgrid-scale energy k_s, and a time scale via:

$$\nu_t = C_M k_s T_s \tag{4}$$

where k_s is estimated by filtering the velocity field, $k_s = \left(\overline{u_i} - \tilde{\overline{u_i}}\right)^2$, where '~' denotes test-filtering, and T_s, the *mixed* time-scale, is defined as a combination of typical large and small time-scales,

$$T_s = \left[\frac{\sqrt{k_s}}{\Delta} + \frac{|S|}{C_T}\right]^{-1} \tag{5}$$

where Δ is the filter width (computed as the cubic-root of the cell volume). The first part is a subgrid time-scale at the cut-off level, while the second part is instrumental in securing the correct decay close to the wall. The model uses two constants: $C_M = 0.05$ and $C_T = 10$. These values arise from an optimisation in fully-turbulent channel flows, and thus may not be suited to transitional flows, especially in boundary layers. Particularly important is the latter constant, which dictates the ratio between the two time-scales.

The dynamic Smagorisky (DSM) variant used herein adopts the least-square method proposed by Lilly [15], in which the Smagorisky constant C is determined from:

$$C = -\frac{1}{2}\frac{L^*_{ij}M_{ij}}{\tilde{\Delta}M_{ij}M_{ij}} \tag{6}$$

where '*' denotes the adjoint of the stress tensor defined as

$$L_{ij} = T_{ij} - \tilde{\tau}_{ij} = \widetilde{\overline{u_i}\,\overline{u}_j} - \tilde{\overline{u}}_i\,\tilde{\overline{u}}_j \tag{7}$$

and

$$M_{ij} = \alpha^2|\tilde{\overline{S}}|\tilde{\overline{S}}_{ij} - \widetilde{|\overline{S}|S_{ij}} \tag{8}$$

where α is the ratio between the test and subgrid filter. In the present applications, the test-filter operations in both models above were performed with the Simpson rule, and filtering was applied only to the plane parallel to the wall. To avoid spurious oscillations and negative values of eddy-viscosity, an additional smoothing operation is required for the DSM model. This is effected by an averaging of ν_t in time, rather than in space, given that the spanwise direction cannot be regarded as being *homogeneous* in the normally understood sense, because of the transition process. However, it was found in test simulations that the type of averaging used had a very marginal influence on the results.

Finally, the WALE model evaluates the eddy viscosity from:

$$\nu_t = C_\omega\Delta^2\frac{\left(B_{ij}B_{ij}\right)}{\left(\overline{S}_i j\overline{S}_i j\right)^{5/2} + \left(B_{ij}B_{ij}\right)^{5/4}} \tag{9}$$

where B_{ij} is the deviatoric part of the square of the velocity-gradient tensor:

$$B_{ij} = \overline{S}_{ik}\overline{S}_{kj} + \overline{\Omega}_{ik}\overline{\Omega}_{kj} - \frac{1}{3}\left(\overline{S}_{mn}\overline{S}_{mn} - \overline{\Omega}_{mn}\overline{\Omega}_{mn}\right) \tag{10}$$

where $\overline{S}_{ij}$ and $\overline{\Omega}_{ij}$ are the strain and rotation-rate tensors, respectively. The constant C_ω in Eq. 9 is here taken as 0.1, which is compatible with the Smagorinsky constant

appropriate to isotropic homogeneous turbulence. All three models were thoroughly tested in periodic channel flows, and the MTS model was found to perform markedly better than the other two at elevated Reynolds numbers and marginal resolution. On the other hand, both this model and the DSM have well-known drawbacks. Thus, the eddy-viscosity computed with the dynamic Smagorinsky coefficient needs to be smoothed in order to avoid excessive point-to-point excursions, associated with the inaccurate estimation of the strain tensor on coarse grids, while the MTS model relies on the definition of two constants (C_M and C_T), which adversely affects its generality.

4 Flat-Plate Boundary Layer

4.1 Visual observations

Reference to Fig. 1 shows that the boundary layer is initially subjected to a favourable streamwise pressure gradient, up to $x/L = 0.3$. This tends to attenuate the effect of the perturbations by reducing their intensity. Beyond $x/L = 0.3$, the boundary layer is subjected to an adverse pressure gradient, which is sufficiently large to provoke separation. This variation is, qualitatively, representative of the pressure gradient on a highly-loaded turbine blade. At low free-stream turbulence, the flow undergoes transition following laminar separation, and the turbulent shear layer then reattaches further downstream, well before the trailing edge.

The process by which the shear layer is destabilized is very sensitive to the Reynolds number, the free-stream-turbulence intensity, the spectral properties of the turbulent free-stream and the domain dimension in the streamwise direction, among others. This subsection provides a first qualitative illustration of the sensitivity of the transition process to the free-stream turbulence level.

Visualizations of the instantaneous streamwise-velocity perturbation $u' = U - u$ for three free-stream-turbulence levels are shown on Fig. 3, with motion faster than the mean velocity shown in light shades (yellow), and slower one in darker shades (blue). Regions of instantaneous reverse flow are indicated as dark grey patches. At $Tu = 0\%$, disturbances set in well beyond the spanwise homogeneous separation location at $x/L = 0.365$, with oblique roller-like structures occurring around $x/L = 0.56$ and resembling varicose modes seen in other free shear layers (e.g. [4]). When the free-stream turbulence increases to $Tu = 1\%$, elongated streamwise structures appear in the separated shear layer, and the separation itself, although still laminar, begins to become irregular in the spanwise direction. This irregularity is indicative of perturbations by Klebanoff modes, given the relatively high free-stream turbulence and the rather thin boundary layer, a conjecture examined later. Streaky regions of higher streamwise velocity are more likely to appear in the separated shear layer, downstream of troughs in the separation line (i.e. dips in the dark-grey patches in Fig. 3b). This early onset of transition is the primary cause for a drastic reduction in the size of the separation bubble. While the shear layer seems to grow monotically downstream of separation for the zero-turbulence case, the visual thickness of the layer appears to reach a plateau from $x/L = 0.7$ onwards at $Tu = 1\%$. For the highest value of Tu (Fig. 3c), the transition occurs very early and is highly non-uniform, with large portions of the flow not even being subjected to a reversal in the near-wall region. Intense streamwise vortices (characterized by alternate positive

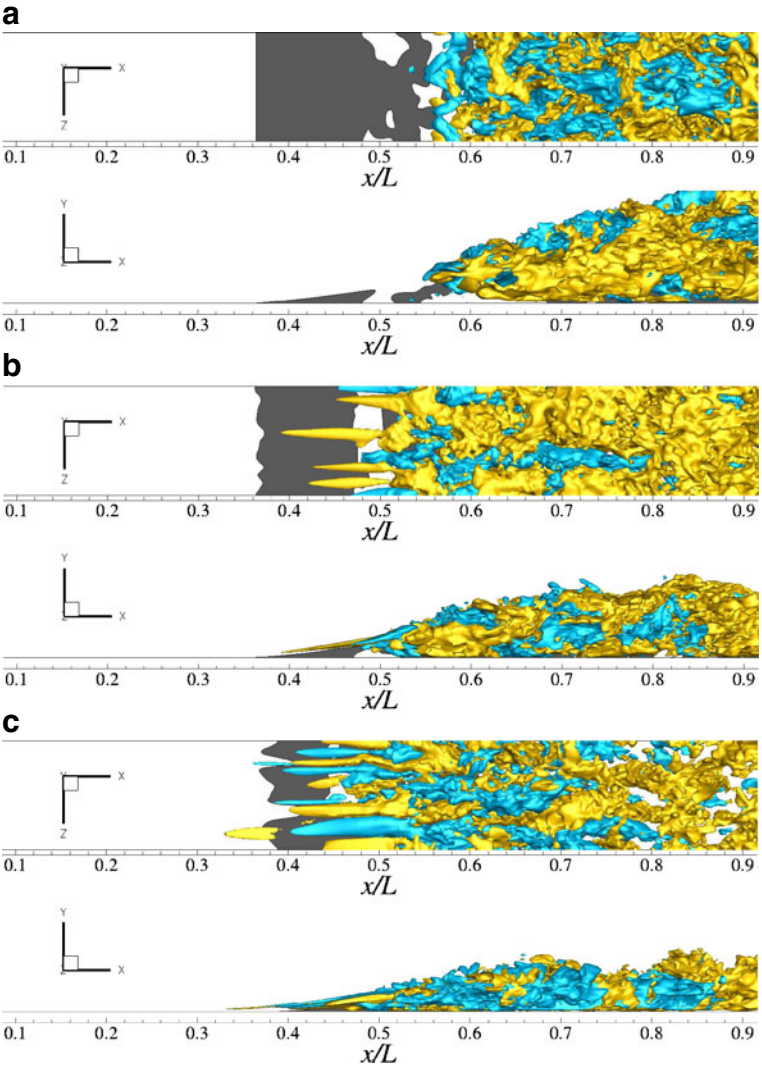

Fig. 3 Flat-plate case: isosurfaces of $u' = \pm 0.2U_0$ for **a** $Tu = 0\%$, **b** $Tu = 1\%$ and **c** $Tu = 2\%$

and negative values of u') are found upstream of separation, and are the footprints of the Klebanoff modes mentioned earlier. The visual thickness of the shear layer is even more reduced, with saturation reached around $x/L = 0.65$.

4.2 Effect of SGS modelling

The above visualisations were obtained with the MTS model, but similar images have been derived from simulations with the other two SGS models, and these need not, therefore, be included herein. The general transition scenario, as described above, is in agreement with previous observations arising from the corresponding DNS

studies. Specifically, the different transition features observed in the previous section accord qualitatively well with the DNS results, including the development of KH instabilities in the unperturbed separated shear-layer, and the growth of Klebanoff modes at higher free-stream-turbulence intensities, with the modes having roughly the correct scale.

However, significant differences between LES and DNS come to light in the statistical analysis. Here, the influence of SGS modelling is assessed for $Tu = 0$ and 1%, for which DNS data are available from Wissink and Rodi [28]. The streamwise variation of several quantities, obtained with the three models summarised in Section 3.3, are shown on Fig. 4. Corresponding mean streamwise velocity and Reynolds-stress profiles are shown on Fig. 5. The skin-friction coefficient C_f converges most slowly and remains rather uneven, despite the long integration time of about 40 time units

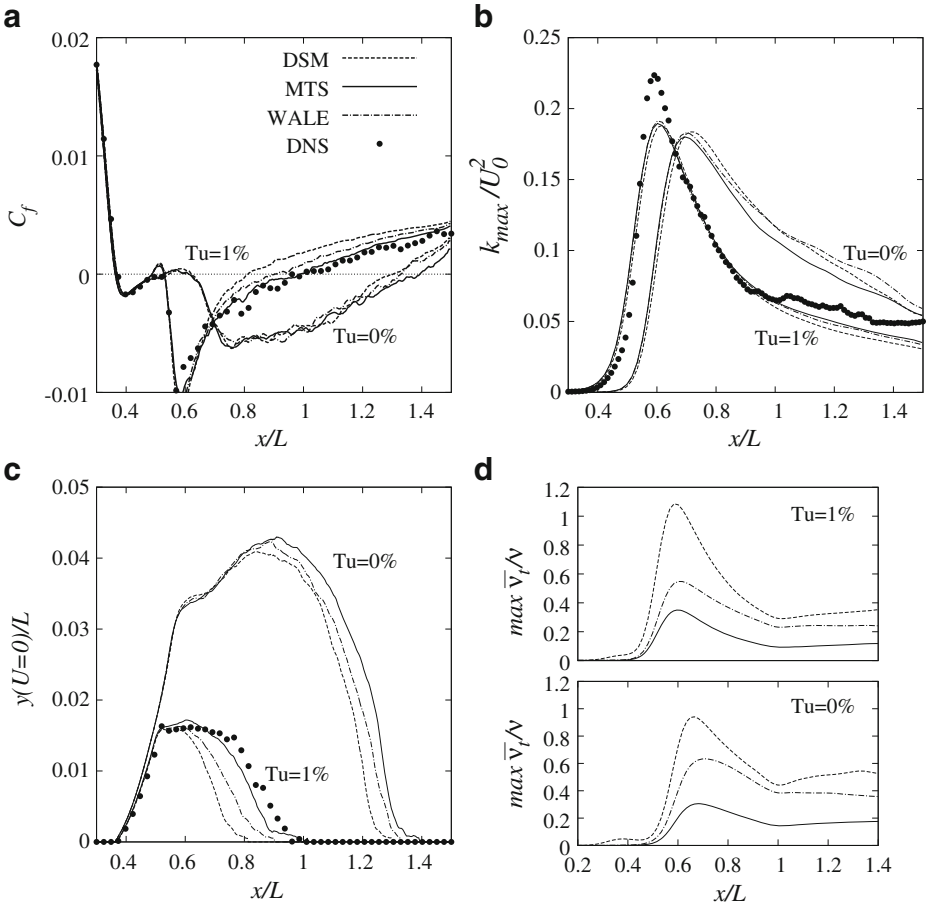

Fig. 4 Flat-plate case: streamwise variations of **a** the skin-friction coefficient C_f, **b** the maximum of the turbulence energy k in the wall-normal direction, **c** the separation bubble half-height (identified as the wall-normal position where the sign of the streamwise velocity changes) and **d** the wall-normal maximum of the SGS viscosity ν_t/ν

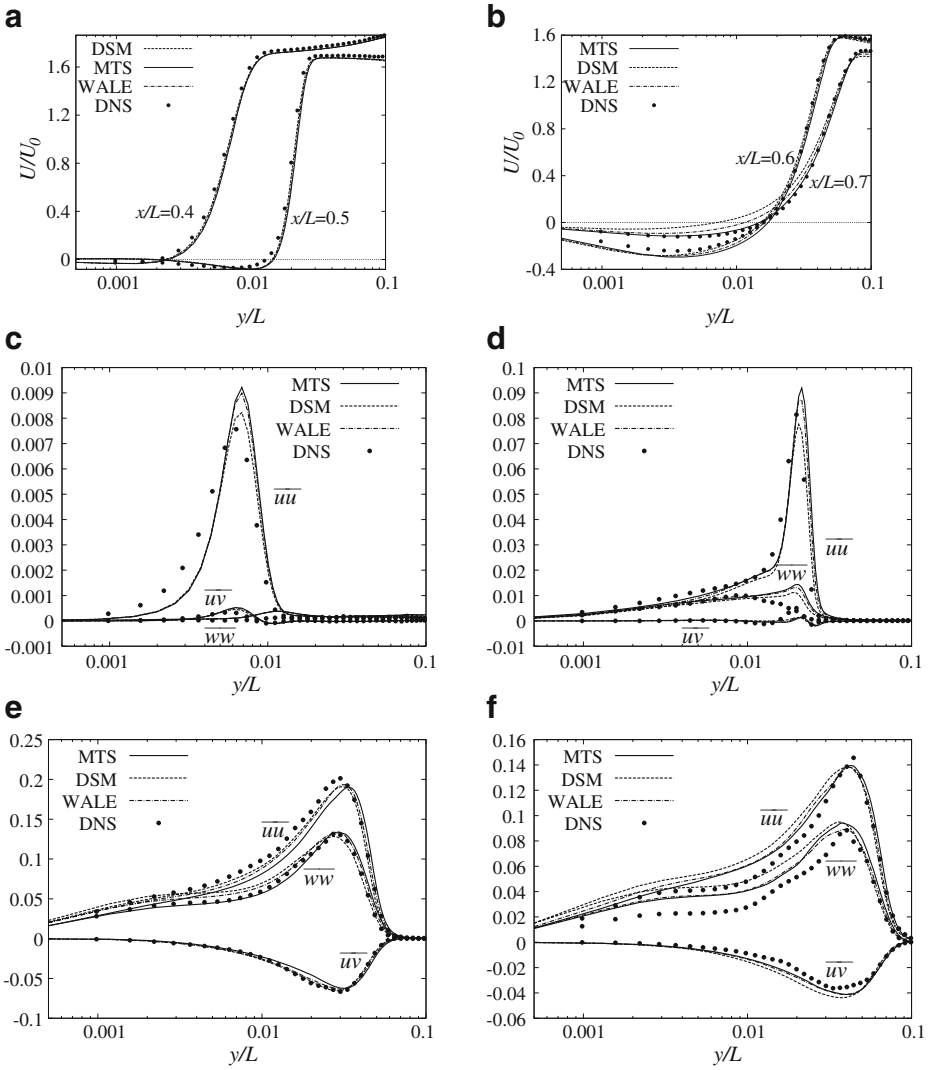

Fig. 5 Flat-plate case: **a**, **b** streamwise velocity profiles at four positions inside the separation bubble, and **c**–**f** Reynolds stress profiles for these same four positions: **c** $x/L = 0.4$, **d** $x/L = 0.5$, **e** $x/L = 0.6$ and **f** $x/L = 0.7$. DNS results from Wissink and Rodi [28] are shown with symbols (•)

L/U_0, or 20 flush-through times. For $Tu = 0\%$, all SGS models give similar variations, with separation at $x/L = 0.365$, and reattachment occurring close to the domain exit, at $x/L = 1.385$. A secondary recirculation bubble is found around $x/L = 0.6$, regardless of the model used. For $Tu = 1\%$, the different SGS models give significant differences in C_f, with the MTS model returning a result closest to DNS, with reattachment occurring in both cases around $x/L = 0.95$, while the DSM model gives the upstream-most reattachment location at $x/L = 0.88$. All models return very similar results in the pre-transitional region, upstream of $x/L = 0.7$.

The evolution of the maximum of turbulence energy k is shown on Fig. 4b. For $Tu = 0\%$, the turbulence energy grows rapidly (*exponentially*) from $x/L = 0.45$, consistent with the inflectional-profile-instability mechanism, until it reaches the linear-growth regime at around $x/L = 0.55$. The turbulence energy then continues to rise until the peak at $x/L = 0.72$, with all three SGS models giving very similar results. A similar behaviour is observed for the higher level of free-stream turbulence, with one major difference, namely that the maximum of turbulence energy is non-zero ahead of separation (reflecting the presence of Klebanoff modes), thus leading to an earlier transition and higher peak of energy in the separation bubble. While the initial growth is well represented by the LES, the peak at $Tu = 1\%$ is underestimated, whatever SGS model is used. However, like the rise, the decay of k downstream of the peak is again gratifyingly well predicted, with insignificant differences between the models.

Figure 4c shows the locus of zero streamwise velocity, and thus identifies the length and (roughly) the half-height of the recirculation bubble. The strong sensitivity of the separated zone to Tu clearly ties closely with the variations of the skin friction, and also the turbulence energy. In the early stage of separation, where the growth of the boundary layer is linear, all models return very simular results, for both values of Tu. Further downstream, once the large-scale structures associated with the KH instability start developing, all models perform equally well for $Tu = 0\%$, which is consistent with their basic function of representing the effects of small-scale features. As might be expected from the skin-friction behaviour, the size of the separation bubble is fairly sensitive to the SGS model for $Tu = 1\%$, in which case the flow is characterized by a much wider range of scales. The best results are obtained, again, with the MTS model, yielding the downstream-most reattachment point, and the highest separation bubble. This is consistent with the results shown on Fig. 4d which demonstrate that the lowest level of averaged eddy-viscosity ratio $\overline{\nu_t}/\nu$ is returned by the MTS model. In all cases, the eddy viscosity reaches its peak at around $x/L = 0.68$ for $Tu = 0\%$ and $x/L = 0.6$, i.e. the same locations as the peak of the maximum of k/U_0^2 in Fig. 5b. In the light of this observation it might be presumed that a zero-eddy-viscosity "model" would also perform well. However, the grid resolution is too coarse to perform such a simulation realistically, in which case the separation bubble does not reattach ahead of the end of the domain for the lower turbulence intensity. Also noticeable is the earlier growth of ν_t/ν returned by the DSM formulation, compared to the other two models, and this is due to the formulation of the model itself; in particular, its greater sensitivity to any strain perturbations, even in laminar conditions.

Profiles of the streamwise velocity U and the Reynolds stresses $\overline{uu}$, $\overline{ww}$ and $\overline{uv}$, for $Tu = 1\%$ only, are compared in Fig. 5 to results extracted from Wissink and Rodi's DNS data. Close to the separation location, $x/L = 0.4$, the second-moment field is strongly dominated by streamwise fluctuations, consistent with Klebanoff modes, with a very low level of shear stress, and almost zero-cross-stream and spanwise components, all in close agreement with the corresponding DNS data. Attention is drawn, however, to the very low level of fluctuations (note the ordinate scale). Further downstream, at around $x/L = 0.5$, saturation is reached, with the separation bubble ceasing to grow, Fig. 4c, while k starts rising. In fact, this is the location where all the minor components, $\overline{vv}$ and $\overline{ww}$, start to rise towards the state characteristic of established turbulence. The most important difference relative to the DNS results is observed in respect of $\overline{ww}$: the peak is predicted around $y/L = 0.008$ in the DNS,

i.e. rather close to the wall, and this is probably associated with fluctuations from the downstream reverse flow, while the peak is predicted at around $y/L = 0.02$ by the LES, in the middle of the free-shear layer. Further downstream, agreement between all LES solutions and the DNS results is much better. Close to the position of maximum energy, in particular, the different models return very different eddy-viscosity ratios (Fig. 6), while at other positions in the separated region, the profiles of $\overline{\nu_t}/\nu$ are similar in shape, albeit with different maxima, the lowest returned by the MTS model.

4.3 Effect of free-stream turbulence

The previous section has shown that all three SGS models return similar predictions of the transition process, given a resolution of about 7.5% of the DNS, in terms of overall mesh size. Of the models, the MTS approximation yields superior agreement with the DNS in the separated region, due to the lower level of eddy viscosity it gives. This model has thus been used to study the dependence of the flow field on the variation of free-stream turbulence within the range 0–2%, recorded at the point of separation. Results for all four cases given in Table 1 are shown on Figs. 7 and 8, with the latter focusing on the early stages of separation.

Consistent with previous results, the size of the separation bubble progressively reduces as Tu increases (Fig. 7). In contrast, the peak turbulence energy declines monotonically, down to a level of only 20% of that at $Tu = 0\%$. This behaviour may be counter-intuitive, but reflects the predominance of KH-type vortices at low Tu levels, while their breakup is enhanced by an increase in Tu. Consistent with this interpretation is the fact that the thickness of separated/reattached shear layer decreases with increasing Tu, thus containing smaller-scale structures.

The reduction of the separation bubble with increasing free-stream turbulence is, predictably, closely linked to the behaviour of the boundary layer upstream of separation. Figure 8 shows the streamwise evolution of Re_θ, δ, the shape factor $H = \delta^*/\theta$ and the maximum of $u_{\rm rms}$ in the wall-normal profile, all in the late stage of attached flow and the early stage of separation (the boundary-layer edge was determined by way of a minimum-vorticity threshold). Corresponding profiles, at three locations upstream of the separation (which occurs in all cases around $x/L =$

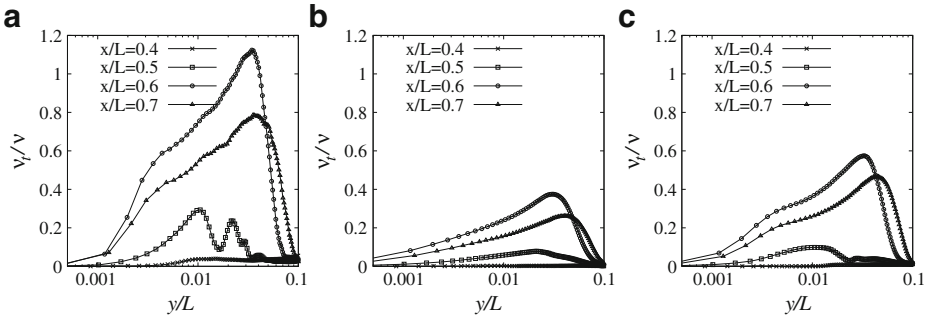

Fig. 6 Flat-plate case: profiles of $\overline{\nu_t}/\nu$ at four different streamwise locations, downstream of separation and upstream of reattachment, for **a** DSM, **b** MTS and **c** WALE models

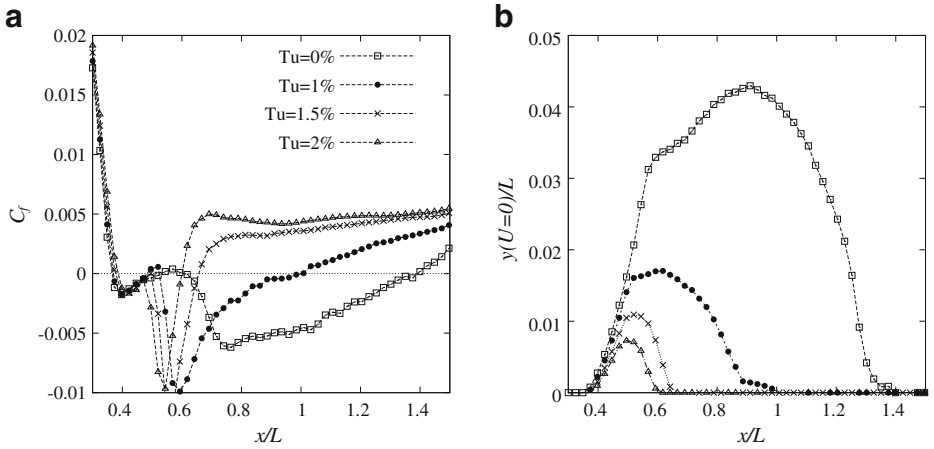

Fig. 7 Flat-plate case: streamwise evolution of **a** the skin-friction coefficient C_f and **b** the separation bubble half-height (identified as the wall-normal position where the sign of the streamwise velocity changes), for various free-stream-turbulence intensities

0.365) are given in Fig. 9. Prior to transition, the momentum thickness is identical for all cases, but then the values start diverging from one another from the point of separation, the momentum thickness increasing with increasing turbulence intensity, due to increased wall friction. The displacement thickness, on the other hand, follows opposite trends, with the lowest curve obtained for $Tu = 2\%$. This is again due to KH vortices, which tend to increase the boundary-layer thickness, but have virtually no effect on momentum loss. As the curves begin to diverge prior to separation, this leads to diverging shape-factor evolutions, before as well as after separation, and such differences in the shape factor play a role in the receptivity of the separated shear layer to external perturbations. A stability analysis by Dovgal et al. [6], using different profiles, shows that the receptivity of an attached boundary layer is very different in a zero-pressure-gradient, Blasius-type profile, and in a profile more akin to that in an accelerated/decelerated boundary layer, expressed in the form of an hyperbolic-tangent formulation. The shape factor H of the present profile in attached conditions is 2.25, while the Blasius profile has the higher shape factor of $H = 2.59$. The present shape factor of 2.25 is associated with a profile that is very stable to 2D disturbances, even at a high Reynolds number. Indeed, it has been shown that this profile shape is even more resistant to 3D disturbances. Alam and Sandham [2] have also shown that hyperbolic-tangent profiles are absolutely unstable if the reverse flow reaches 15% of the free-stream velocity. In the present cases, this criterion is reached only for $Tu = 0\%$ and $Tu = 1\%$.

Very few studies report the growth of perturbations in the boundary layer prior to separation (e.g. [13]). The mechanisms found here are similar to those observed in a very recent simulation by McAuliffe and Yaras [18]. In both cases, the streaks originate close to the leading-edge of the flat plate. Alam and Sandham [2] reported the creation of Λ-type vortices in the separation bubble, which are the result of instability mechanisms occurring in the separated shear layer only, but do not report on the growth of Klebanoff-mode instabilities before separation. This is a major

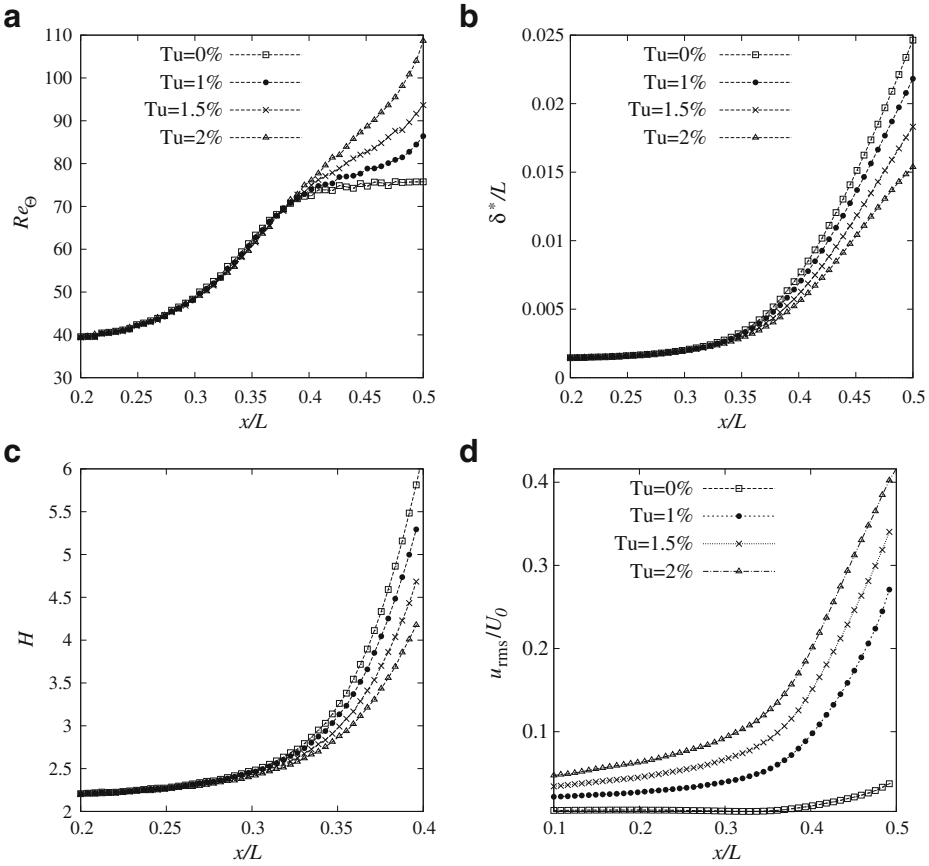

Fig. 8 Streamwise vatriations of **a** the momentum-thickness Reynolds number θ, **b** the displacement thickness δ^*, **c** the shape factor $H = \delta^*/\theta$ and **d** the maximum rms of the streamwise fluctuations in the wall-normal profiles in the attached boundary layer upstream of separation

difference between these two studies: in the latter study, a Blasius-type boundary layer is imposed at the inlet, the flow is not computed from its inception, and it is thus less receptive to free-stream disturbances.

Figure 8d clearly shows different levels of receptivity by the interaction between Tu and the Klebanoff modes. Thus, the streamwise fluctuations upstream of separation grow at very different rates in the attached boundary layer, depending on the level of free-stream turbulence, but then at very similar rates shortly after separation. The growth rate is proportional to $Tu \times \sqrt{x/L}$ (consistent with the linear regime, Brandt et al. [3]), and is exponential in the separated region. The profiles of $\overline{uu}$ (Fig. 9) confirm this behaviour, and also indicate that the streaks associated with the Klebanoff modes develop at the same distance from the wall irrespective of the value of Tu, with a peak around $y/\delta^* = 1.3$, similar to that found in Brandt et al. [3]. Crucially, the case $Tu = 0\%$ does not show this peak, since no instability is observed upstream of separation in the absence of free-stream disturbances. Another interesting feature comes to light when examining the normalized vorticity profiles

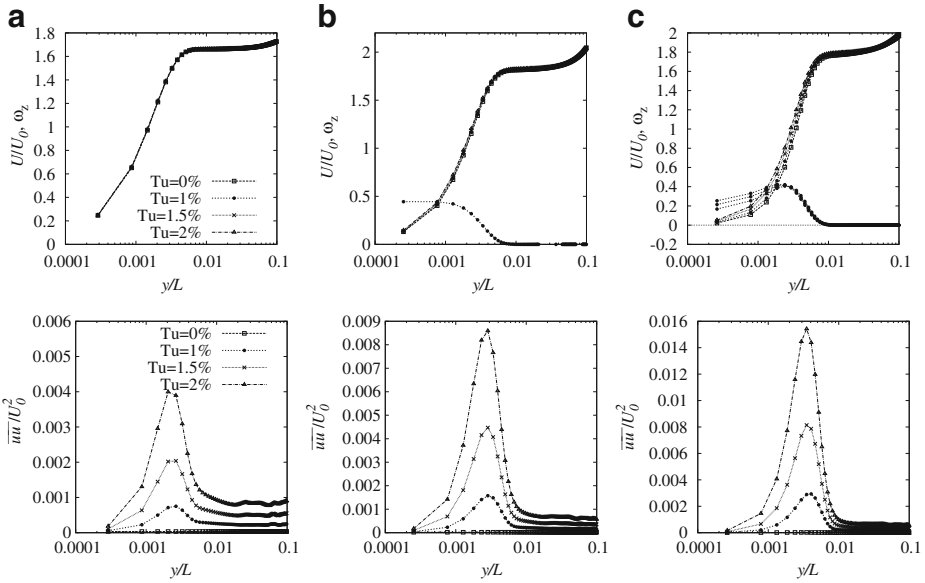

Fig. 9 Flat-plate case: profiles of streamwise-velocity, spanwise vorticity ($Tu = 1\%$ only) and streamwise-velocity fluctuations for **a** $x/L = 0.2$, **b** $x/L = 0.3$ and **c** $x/L = 0.35$

in Fig. 9: the inflection point of an ordinary boundary layer is located at the wall. However, as the boundary layer approaches separation, the inflection point, characterized by a maximum of dU/dy away from the wall, is at around $y/L = 0.003$. This is also the location at which u_{rms} reaches a maximum. The presence of this inflection point explains the exponential growth observed in Fig. 8d before the flow separates.

4.4 Effect of free-stream spectrum

The transition scenario described above was based on simulations where the free-stream field contains a broad-band spectrum of fluctuations. In attached flows, the transition process is known to be selectively receptive to particular segments of the wave-length spectrum, with Klebanoff modes sensitive to the larger wave lengths, while shorter wave length (higher frequencies) interact, principally, with the smaller scales that arise from the breakdown of large vortices as the transition progresses towards established turbulence. No such sensitivity has been reported in the case of turbulent separated shear layers, however, and most of the stability analyses focus on the early part of the separation, with very little being reported on the effects of free-stream wave lengths in the latter part of the flow.

This section reports results from two simulations with the two spectra given, respectively, by Eqs. 1 and 2, but for one case only, namely $Tu = 1\%$; other cases show a similar behaviour, or do not display features of particular interest. For the fixed free-stream turbulence level, the same peak wave number was used in the generation of the two perturbation fields, but with different decay characteristics in the high-frequency range. Given the two spectra as specified, there are now two

options, namely to prescribe a fixed integral of the energy (i.e. the integral of the spectrum), or to fix the energy at the peak wave number. The former approach was chosen here, because it gives roughly the same decay ahead of the leading edge (Fig. 10a).

The main difference between the two cases occurs, remarkably, in the later stage of the separation bubble, downstream of $x/L = 0.6$. Further upstream, the interaction with the free stream proceeds primarily within the large-scale portion of the spectrum, and the properties of both spectra are fairly similar at low wave numbers. It is only once the separated shear layer contains a significant proportion of small-scale structures that the flow is influenced by higher wave-number portions of the spectra.

Figure 10b–d give selected results which illustrate the sensitivity of the flow to the variation in the spectrum. An important general observation made first is that

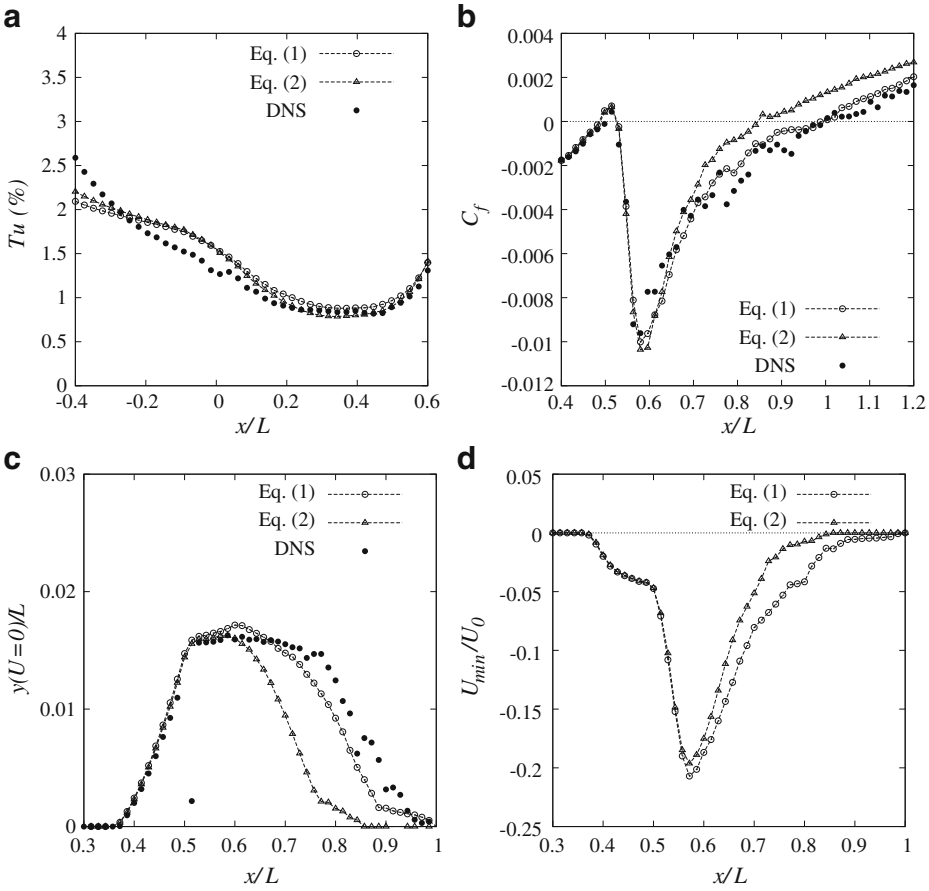

Fig. 10 Flat-plate case: streamwise variations of **a** decay of free-stream turbulence intensity, **b** the skin-friction coefficient, **c** the height of the reverse-flow layer and **d** minimum reverse streamwise velocity, for the two spectra investigated, Eqs. 1 and 2, at the same free-stream-turbulence intensity at inlet

certain aspects of the transition process are evidently quite sensitive to the free-stream spectrum, and this poses obvious uncertainties when predictions are made without spectral information being available. Second, Fig. 10 shows that the rear of the separation zone is particularly strongly affected, with the narrower spectrum resulting in a faster recovery from separation and a shorter and thinner recirculation zone. The origins of this sensitivity are difficult to identify. It is possible that the higher peak of energy in the narrower spectrum, which is located at a moderately high wave number, has an especially strong influence on the shear-layer region in which the large scales are progressively breaking down into smaller scales. It appears that the high wave-number scales present in the von Kàrmàn spectrum, but absent from the narrower spectrum, are less influential. It is also likely that resolution and SGS modelling have disproportionate effects on the high wave-number range, so that the tail of the von Kármán spectrum is not correctly propagated by the LES.

5 Compressor Blade

This section extends the investigation of the flat-plate flow to the compressor blade shown in Fig. 1b. The scope of the extended study is narrower, however, if only because the results derived from it do not offer the level of fundamental insight that was derived from the LES of the flat-plate case. The primary outcome here is a statement on the level of departure of the LES from the DNS solutions, given that the LES mesh size is only 7.5% of that of the DNS. Results are presented for two subgrid-scale models and for two values of free-stream-turbulence intensity, namely $Tu = 0\%$ and 3.25%, prescribed at the DNS inlet plane.

Isosurfaces of the Q-criterion, on both the pressure and suction sides, are shown in Fig. 11, for the higher free-stream-turbulence level, obtained with the MTS subgrid-scale model. These images are, qualitatively, in very good agreement with observations by Zaki et al. [34], made in the light of their DNS results. On the suction side, an extensive streamwise region of elongated low- and high-speed streaks is observed upstream, followed further downstream by flow separation and spanwise-oriented structures associated with KH modes and subsequent breakdown. On the pressure side, transition to turbulence occurs much earlier, with elongated structures preceding a rapid breakdown to turbulence, akin to that observed in a canonical, attached boundary layer undergoing bypass transition.

The transitional features on both sides of the compressor blade clearly differ substantially. On the pressure side, both elements of natural and bypass transition are observed, and the flow remains attached when the free-stream-turbulence intensity is elevated. On the suction side, Klebanoff modes are damped due to the favourable pressure gradient, but do not vanish. This is followed by a long separated region in the aft part of the blade.

As stated in the introduction, the same inflow perturbations as in the DNS have been used in the present LES (albeit interpolated). The streamwise decay of the free-stream-turbulence intensity, Tu, measured along the mid-pitch line between suction and pressure surfaces, and defined as $Tu = \sqrt{2k/3(U^2 + V^2)}$, is shown in Fig. 12. The initial decay rate is much higher than that observed in the DNS, but due to the shortened inlet region in the LES (-0.4 as opposed to -0.5 of chord), Tu reaches the DNS value at about $x/L = -0.2$, and the two remain close until the end of the

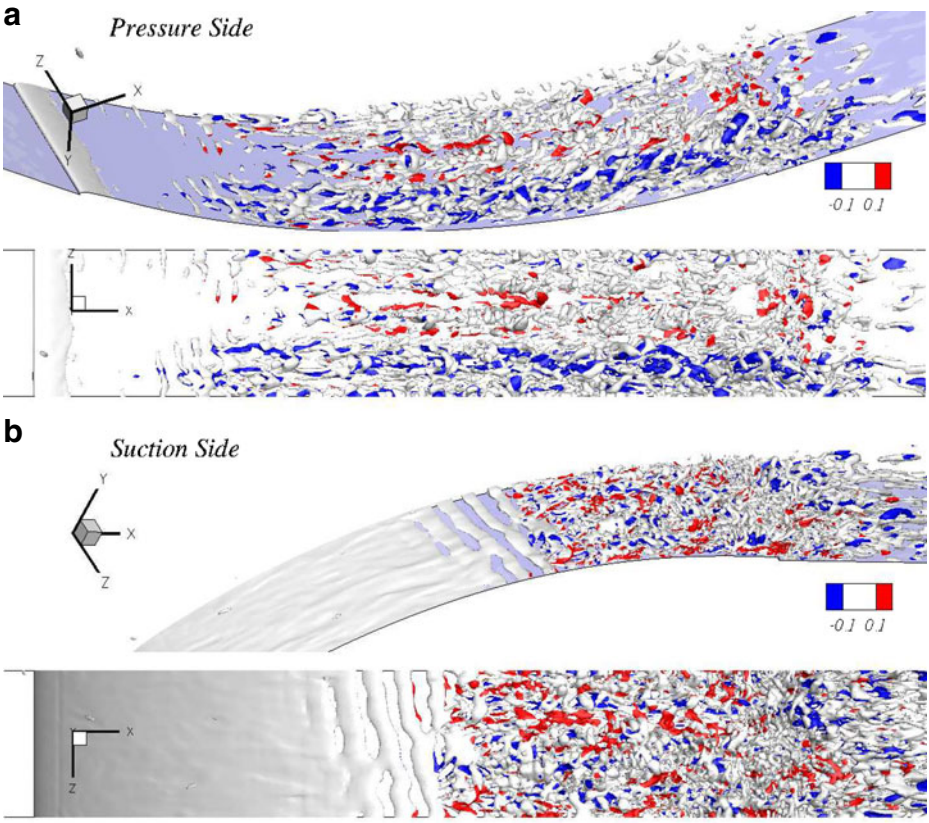

Fig. 11 Compressor blade: perspective and top views of isosurfaces of the Q-criterion on **a** pressure side and **b** suction side, for $Tu = 3.25\%$, colored by the streamwise velocity fluctuations ($-0.1 < u'/U_{in} < 0.1$)

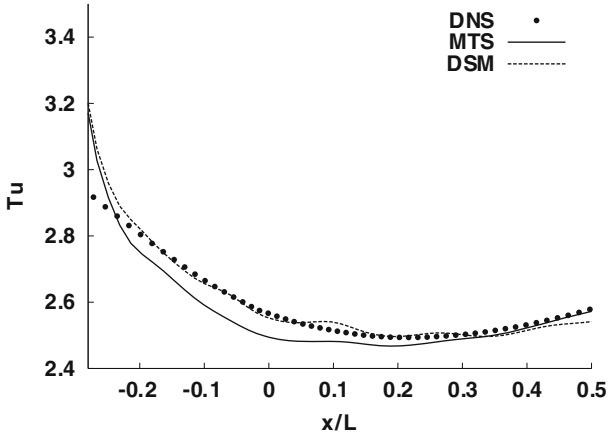

Fig. 12 Compressor blade: streamwise variation of the free-stream-turbulence intensity Tu for the turbulent case ($Tu = 3.25\%$)

blade passage ($x/L = 1$). The decay rate obtained with the MTS model matches closely that of the DNS, while the DSM model gives slightly higher values in the passage.

A comparison of LES results obtained with the MTS model with corresponding DNS results is shown in Figs. 12, 13 and 14. In transitional flows, the SGS model must not corrupt the laminar portion of the flow by introducing spurious dissipation, and this is one of the issues examined below.

Figure 13a and b shows the pressure coefficient C_p for the inlet turbulence intensities $Tu = 0$ and 3.25%, respectively. For the latter case, results obtained with both SGS models are in good agreement with the DNS results. When the inlet forcing is absent, however, the MTS model performs markedly better, especially on the suction side, where the strong pressure drop in the separated region is correctly predicted (albeit with a slight delay). On the other hand, neither SGS model captures correctly the modest separation region on the pressure side, identified by the pressure plateau in the DNS variation, but this may simply reflect poor resolution.

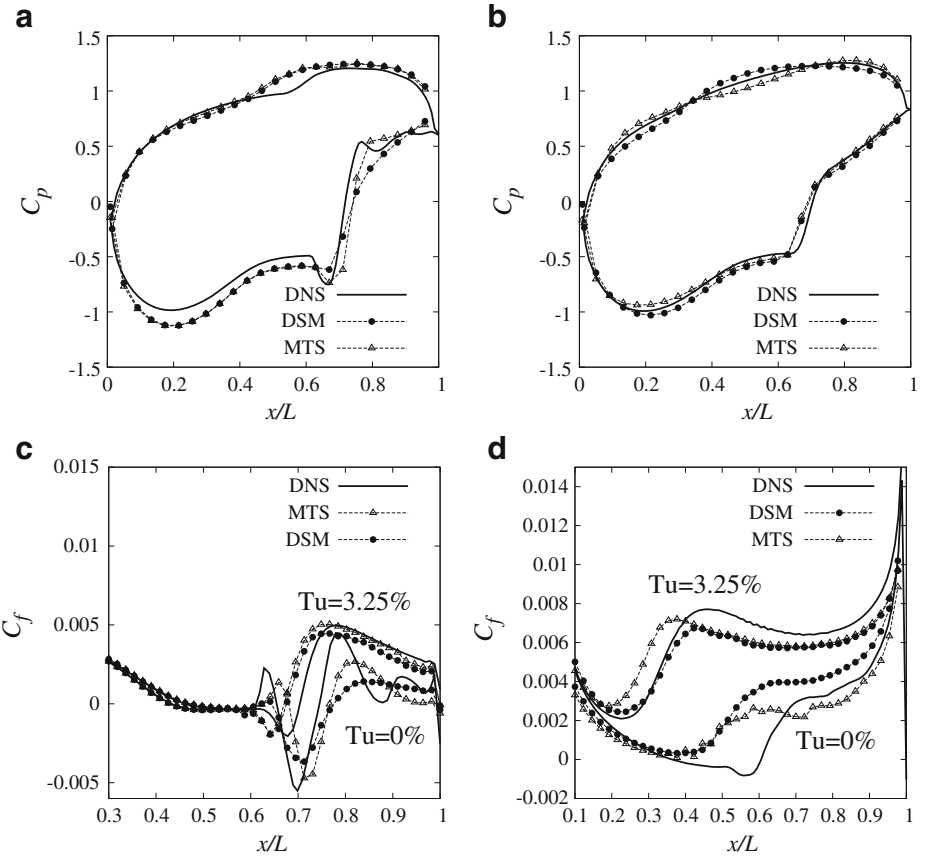

Fig. 13 Compressor case: streamwise variations of the pressure coefficient $C_p = (p_0 - p)/(p_0 - p_s)$ for **a** $Tu = 0\%$ and **b** $Tu = 3.25\%$, and of the skin-friction coefficient C_f for **c** suction side and **d** pressure side

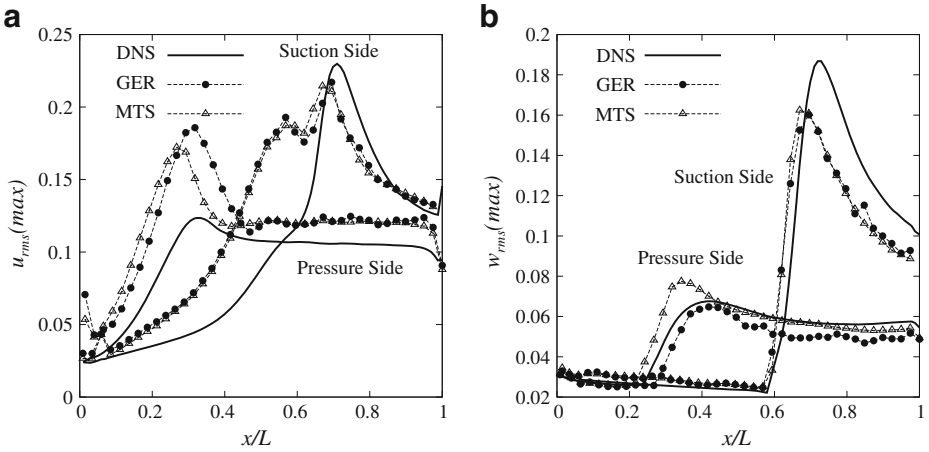

Fig. 14 Streamwise variation of the wall-normal maximum of **a** u_{rms} and **b** w_{rms}, inside the boundary layer on the suction and pressure side, for $Tu = 3.25\%$

The skin-friction coefficient C_f, Fig. 13c, shows (based on the DNS solution) a complex separation scenario on the suction side, especially in the absence of inlet turbulence: the flow detaches around $x/L = 0.43$, and a secondary separation bubble is created between $x/L = 0.63$ and $x/L = 0.68$. Only the MTS model predicts this double-separation behaviour, due to the very low level of eddy viscosity it returns in this region. This model is also returning a fair prediction of the principal downstream separation bubble. At $Tu = 3.25\%$, there is a single separation bubble, and both models return a similarly fair representation of the position of separation and the variation of the skin friction. As noted already, both models fail to capture the separation on the pressure side, and this is confirmed by Fig. 13d. Here too, however, the MTS model performs better, albeit only beyond $x/L = 0.7$.

The streamwise evolution of the peaks of the streamwise and spanwise RMS fluctuations in the boundary layer, on both pressure and suction sides, is shown in Fig. 14, for the case $Tu = 3.25\%$. Upstream of separation, on the suction side, and along the entire pressure side, the LES predicts far too high levels of streamwise-velocity fluctuations. In this region, the maximum value is in the boundary layer. In near-wall shear layers, insufficient resolution is well known to result in excessive streamwise intensity and anisotropy, and it may well be that the defects observed here have the same origin. Nevertheless, both SGS models reproduce the early increase in fluctuations, downstream of the leading edge, especially on the pressure side, where the perturbations in the boundary layer tend to rise quickly, but then decrease as turbulence sets in and the anisotropy decreases dramatically. This early amplification is consistent with the higher levels of wall-normal perturbations in the passage predicted by the LES relative to the DNS (not included). These wall-normal perturbations are directly linked to the amplification of laminar streamwise streaks in the boundary layer. Once separation sets in, the LES predicts a turbulence level that matches closely that resulting from the DNS. The maximum spanwise intensity is fairly well represented, despite the coarser resolution, and this lower sensitivity to resolution is also observed in boundary layers and channel flow.

6 Conclusions

An overall conclusion emerging from the study is that LES yields a *credible* representation of transition that is provoked, or promoted, by a combination of free-stream turbulence and separation, at a small fraction of the computational resources needed for a full DNS resolution – the default approach to resolving transition. However, there is clearly a price to pay, in terms of the level of fidelity, arising from the much coarser resolution and the use of subgrid-scale modelling.

The study has focused primarily on the fundamentally interesting case of separation from a flat plate, with emphasis being placed on the sensitivity of the representation of transition to subgrid-scale modelling, free-stream turbulence and the spectral representation of the later. Unlike most previous studies, the processes around the leading edge are resolved, as this is placed downstream of the inlet plane. Results for this case show that the transition behaviour is predicted realistically, compared with available DNS data. In particular, (i) the sensitivity of the separation bubble, in terms of its extent and strength, to the free-stream turbulence is returned broadly correctly; (ii) the formation of the Klebanoff modes upstream of separation is captured; and (iii) the velocity and Reynolds stresses are correctly predicted. The main discrepancies arise in the early stage of transition in the separation bubble, where the level of SGS eddy viscosity rises, while the flow cannot yet be considered as being turbulent. This is due to high unsteady straining in the unstable, though not turbulent, region. The result is a somewhat shorter separation bubble than that predicted by the DNS. The level of this shortfall depends on the subgrid-scale model used, the dynamic Smagorinsky model performing worst, and the Mixed-Time Scale returning the best agreement with the DNS data, due to the lower subgrid-scale viscosity it returns. It is also shown that the transition behaviour is sensitive to the details of the perturbations (i.e. the energy spectra and peak of energy). However, this could not be confirmed by reference to DNS, because of the absence of data. From a dynamical perspective, all three models give results which are consistent with previous theoretical and numerical analyses, specifically in respect of the growth of fluctuations, akin to Klebanoff modes, ahead of separation at high free-stream-turbulence intensity, which consequently leads to a faster breakdown of the Kelvin–Helmholtz vortices in the initial stage of the separated region. The energy carried by the Klebanoff modes increases with the free-stream-turbulence intensity, and thus leads to a greater reduction in the separation-bubble length.

A more restricted study of a compressor blade has brought to light that additional geometric complexity increases the challenge posed to LES when required to reproduce the fully-resolved flow physics. This is especially so at very low free-stream turbulence, in which case the LES results are very sensitive to subgrid-scale modelling. Thus, only the mixed-time-scale model, giving the lowest subgrid-scale stresses, captures the double-separation and reattachment process on the suction side, and this also returns a fair representation of both pressure and skin friction at and following separation and transition. However, none of the LES solutions resolves the modest separation zone predicted by the DNS on the pressure side, on which the transition scenario is very different from that on the suction side. At a high level of free-stream turbulence, the sensitivity to subgrid-scale modelling is much lower, and both models predict the DNS pressure and skin friction fairly well. Visualisations show that the LES is able to capture the streaky structure of the pre-transitional boundary layer, again associated with the Klebanoff modes. The visualisation also

bring to light the rapid formation of spanwise structures upon separation, which are also observed on the flat plate. While the LES solutions predict the decay of the free-stream turbulence fairly well, the anisotropy is significantly over-estimated, with the streamwise intensity being much too high upstream of transition. This is primarily a reflection of poor resolution. The resolution defects upstream of separation have a particularly strong effect on the transition on the pressure side, on which bypass transition occurs in the attached boundary layer as a consequence of non-linear growth of the Klebanoff-type perturbations. Thus, transition is provoked too early, especially at zero inlet turbulence, and separation is prevented at mid-chord by the high level of turbulence predicted by the LES.

References

1. Abdalla, I., Yang, Z.: Numerical study of the instability mechanism in transitional separating-reattaching flow. Int. J. Heat Fluid Flow **25**(4), 593–605 (2004)
2. Alam, M., Sandham, N.: Direct numerical simulation of 'short' laminar separation bubbles with turbulent reattachment. J. Fluid Mech. **410**, 1–28 (2000)
3. Brandt, L., Schlatter, P., Henningson, D.: Transition in boundary layers subject to free-stream turbulence. J. Fluid Mech. **517**, 167–198 (2004)
4. Comte, P., Lesieur, M., Lamballais, E.: Large-and small-scale stirring of vorticity and a passive scalar in a 3-D temporal mixing layer. Phys. Fluids A: Fluid Dyn. **4**, 2761 (1992)
5. Dahlström, S.: Large Eddy Simulation of the Flow Around a High-lift Airfoil. Ph.D. thesis, Department of Thermo and Fluid Dynamics, Chalmers University of Technology (2003)
6. Dovgal, A., Kozlov, V., Michalke, A.: Laminar boundary layer separation: instability and associated phenomena. Prog. Aerosp. Sci. **30**(1), 61–94 (1994)
7. Fasel, H., Postl, D.: Interaction of separation and transition in boundary layers: direct numerical simulations. In: IUTAM Symposium on Laminar-Turbulent Transition, pp. 71–88. Springer, New York (2006)
8. Fishpool, G., Leschziner, M.: Stability bounds for explicit fractional-step schemes for the Navier-Stokes equations at high Reynolds number. Comput. Fluids **38**(6), 1289–1298 (2009)
9. Germano, M., Piomelli, U., Moin, P., Cabot, W.: A dynamic subgrid-scale eddy viscosity model. Phys. Fluids A: Fluid Dyn. **3**, 1760 (1991)
10. Hilgenfeld, L., Pfitzner, M.: Unsteady boundary layer development due to wake passing effects on a highly loaded linear compressor cascade. J. Turbomach. **126**, 493 (2004)
11. Hodson, H., Howell, R.: Bladerow interactions, transition, and high-lift aerofoils in low-pressure turbines. Annu. Rev. Fluid Mech. **37**, 71–98 (2005)
12. Inagaki, M., Kondoh, T., Nagano, Y.: A mixed-time-scale SGS model with fixed model-parameters for practical LES. J. Fluids Eng. **127**, 1 (2005)
13. Jones, L., Sandberg, R., Sandham, N.: Stability and receptivity characteristics of a laminar separation bubble on an aerofoil. J. Fluid Mech. **648**, 257–296 (2010)
14. Lardeau, S., Leschziner, M., Li, N.: Modelling bypass transition with low-Reynolds-number nonlinear eddy-viscosity closure. Flow Turbul. Combust. **73**(1), 49–76 (2004)
15. Lilly, D.: A proposed modification of the Germano subgrid-scale closure method. Phys. Fluids A: Fluid Dyn. **4**, 633 (1992)
16. Lou, W., Hourmouziadis, J.: Separation bubbles under steady and periodic-unsteady main flow conditions. J. Turbomach. **122**, 634 (2000)
17. Marxen, O., Lang, M., Rist, U., Levin, O., Henningson, D.: Mechanisms for spatial steady three-dimensional disturbance growth in a non-parallel and separating boundary layer. J. Fluid Mech. **634**, 165–189 (2009)
18. McAuliffe, B., Yaras, M.: Transition mechanisms in separation bubbles under low-and elevated-freestream turbulence. J. Turbomach. **132**, 011004 (2010)
19. Michelassi, V., Wissink, J., Frohlich, J., Rodi, W.: Large-eddy simulation of flow around low-pressure turbine blade with incoming wakes. AIAA J. **41**(11), 2143–2156 (2003)
20. Monokrousos, A., Brandt, L., Schlatter, P., Henningson, D.: DNS and LES of estimation and control of transition in boundary layers subject to free-stream turbulence. Int. J. Heat Fluid Flow **29**(3), 841–855 (2008)

21. Nicoud, F., Ducros, F.: Subgrid-scale stress modelling based on the square of the velocity gradient tensor. Flow Turbul. Combust. **62**(3), 183–200 (1999)
22. Ossia, S., Lesieur, M.: Large-scale energy and pressure dynamics in decaying 2D incompressible isotropic turbulence. J. Turbul. **2**(13), 1–34 (2001)
23. Pauley, L., Moin, P., Reynolds, W.: The structure of two-dimensional separation. J. Fluid Mech. **220**, 397–411 (1990)
24. Rhie, C., Chow, W.: Numerical study of the turbulent flow past an aerofoil with trailing edge separation. AIAA J. **21(11)**, 1525–1532 (1983)
25. Roberts, S., Yaras, M.: Large-eddy simulation of transition in a separation bubble. J. Fluids Eng. **128**, 232 (2006)
26. Spalart, P., Strelets, M.: Mechanisms of transition and heat transfer in a separation bubble. J. Fluid Mech. **403**, 329–349 (2000)
27. Wissink, J., Rodi, W.: DNS of a laminar separation bubble in the presence of oscillating external flow. Flow Turbul. Combust. **71**(1), 311–331 (2003)
28. Wissink, J., Rodi, W.: Direct numerical simulations of transitional flow in turbomachinery. J. Turbomach. **128**, 668 (2006)
29. Wu, X., Durbin, P.: Boundary layer transition induced by periodic wakes. J. Turbomach. **122**, 442 (2000)
30. Yang, Z., Voke, P.: Large-eddy simulation of boundary-layer separation and transition at a change of surface curvature. J. Fluid Mech. **439**, 305–333 (2001)
31. Zaki, T., Durbin, P.: Mode interaction and the bypass route to transition. J. Fluid Mech. **531**, 85–111 (2005)
32. Zaki, T., Durbin, P.: Continuous mode transition and the effects of pressure gradient. J. Fluid Mech. **563**, 357–388 (2006)
33. Zaki, T., Durbin, P., Wissink, J., Rodi, W.: Direct Numerical Simulation of By-pass and Separation-Induced Transition in a Linear Compressor Cascade. ASME (2006)
34. Zaki, T., Durbin, P., Wissink, J., Rodi, W.: Direct numerical simulations of transition in a compressor cascade: the influence of free-stream turbulence. J. Fluid Mech. **665**, 57–98 (2010)